Citric Acid Enable Morphological Optimization of $Ni_3(PO_4)_2$ Next Generation High Performance Hybrid Supercapacitors

*Mohsenah H. J. Mashniwi[1], Muhammad Saqib[2], Ali Asghar[*2], Majed Y A Almashnowi[3], Faris Alfifi[3], Shahir Hussain[4], Muneerah Alomar[5], Noorjahan Abdul Azees[6], Muhammad Shahid Rashid[*7]*

[1]Department of Physics, Faculty of Sciences, King Khalid University, P. O. Box 9004, 61421, Abha, Kingdom of Saudi Arabia
[2]Additive Manufacturing Institute, Shenzhen University, Shenzhen, China
[3]Department of Physical Sciences, Chemistry Division, College of Science, Jazan University, P.O.Box. 114, Jazan 45142, Kingdom of Saudi Arabia
[4]Department of electrical and electronics engineering, college of engineering and computer science, Jazan University, P.O.Box. 114, Jazan 45142, Kingdom of Saudi Arabia
[5]Department of Physics, College of Science, Princess Nourah bint Abdulrahman University, P. O. Box 84428, Riyadh 11671, Saudi Arabia.
[6]Department of Mathematics, College of Science, Jazan University, P.O. Box 277, Jazan 45142, Saudi Arabia
[7]Department of Physical Sciences, Physics Division, College of Science, Jazan University, P.O.Box. 114, Jazan 45142, Kingdom of Saudi Arabia

Corresponding author Email: mrashid@jazanu.edu.sa (MS Rashid), aliasghar504786@gmail.com (A Asghar)

1. Structure Characterization

The samples crystal phase examination was observed by X-ray diffraction (XRD, TTR-III, Rigaku, Japan). Surface morphology and elemental mapping were studied using field-emission scanning electron microscopy (FE-SEM) and energy-dispersive X-ray spectroscopy (EDS). X-ray photoelectron spectroscopy (XPS; K-Alpha, Thermo Scientific, UK) measures the oxidation and elemental composition. Barrett-Joyner-Halenda (BJH) analysis and Brunauer-Emmett-Teller (BET) theory, that included N_2 desorption-adsorption data, were used to calculate the specific area of surface and pore dimension distributions.

2. Electrochemical Measurements

The electrochemical measurements, consisting of cyclic voltammetry (CV) (scan rate (SR) of 3 to 80 mV s−1), Galvanostatic Charging/Discharging (GCD) (current density (CD) of 1 to 15 A/g), and electrochemical impedance spectroscopy (EIS) (frequency was 10 to 102

kHz), of a single bulk electrode, were studied utilizing a 3-electrode system in a 2 M KOH electrolytic solution through (CHI660E, China). The working electrodes were deposited on NF, while the counter and reference electrodes were a Pt plate and Hg/HgO. The capacitance values, such as gravimetric capacitance and Capacity through CV and GCD of the electrodes, were calculated utilizing the following Eq. (S1-S4)[1]:

$$Csc\ ({}^{F}/_{g}) = \frac{\int_{v_i}^{v_f} I \times V\, dV}{m * s * \Delta V} \quad \text{(S1}$$

$$Csq\ ({}^{C}/_{g}) = \frac{\int_{v_i}^{v_f} I \times V\, dV}{m * s} \quad \text{(S2}$$

$$Ssc = \frac{I \times \Delta t}{A * \Delta V} \quad \text{(S3}$$

$$Ssq = \frac{I \times \Delta t}{m} \quad \text{(S4}$$

Here, specific capacitance (Csc) and capacity (Csq) are calculated by CV. The integral part represents the area of a polygon, m is the deposit mass, s is the SR, and ΔV exhibits the potential window. The GCD profile measures the specific capacitance (Ssc) and capacity (Ssq). I, delta t, and m represent the CD, discharging time, and active mass loading on the electrode, respectively.

The NPCA0.5 was assembled into an asymmetric supercapacitor (ASC) device with NF as a current collector and filter paper as the separator. The electrochemical activity assembled ASC was also evaluated in the same workstation with a 2-electrode setup. The following Eqs. (S5 and S6) are utilized to measure the specific energy (SE), and specific power (SP), accordingly [2]:

$$SE = \frac{1}{2 * 3.6} Ssc(\Delta V)^2 \quad \text{(S5}$$

$$SP = \frac{3600 * SE}{t} \quad \text{(S6}$$

Here, ΔV and t represented the potential window, and time of discharging, accordingly.

3. Fabrication of Asymmetric Supercapacitor

An asymmetric SC device was constructed utilizing electrodes made of NPCA0.5 for the cathode and activated carbon for the anode. Whatman 1 filter paper was employed as a separator among the electrodes. The assembly was subsequently encased in paraffin film to achieve a functional gadget. The electrochemical examination of the constructed gadget was performed in a 2 M KOH aqueous solution. The amount of weight on each electrode in the device is balanced using the Es. S7.

$$m^+C^+V^+ = m^-C^-V^- \quad \text{(S7}$$

C+ and C- (F/g) define the Csc m+ and m-, while (g) signifies the active mass of the cathode and anode materials, accordingly. The mass of AC in the anode is 2 mg.

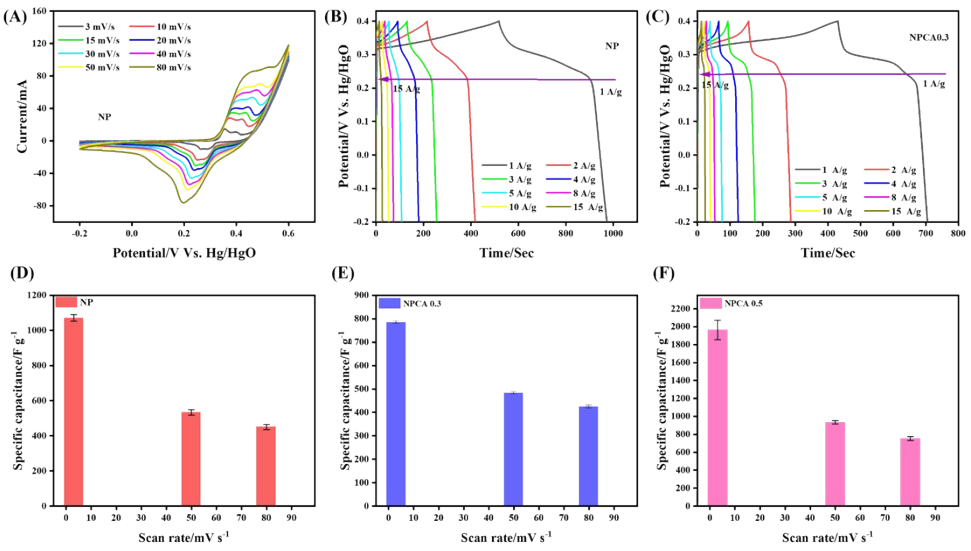

Fig. S1: (A) CV analysis of NPCA and GCD analysis of (B) NPCA and (C) NPCA0.3 and (D-E) Specific capacitance with standard deviation bar chart of prepared electrodes at 3, 50, 80 mV/s scan rates.

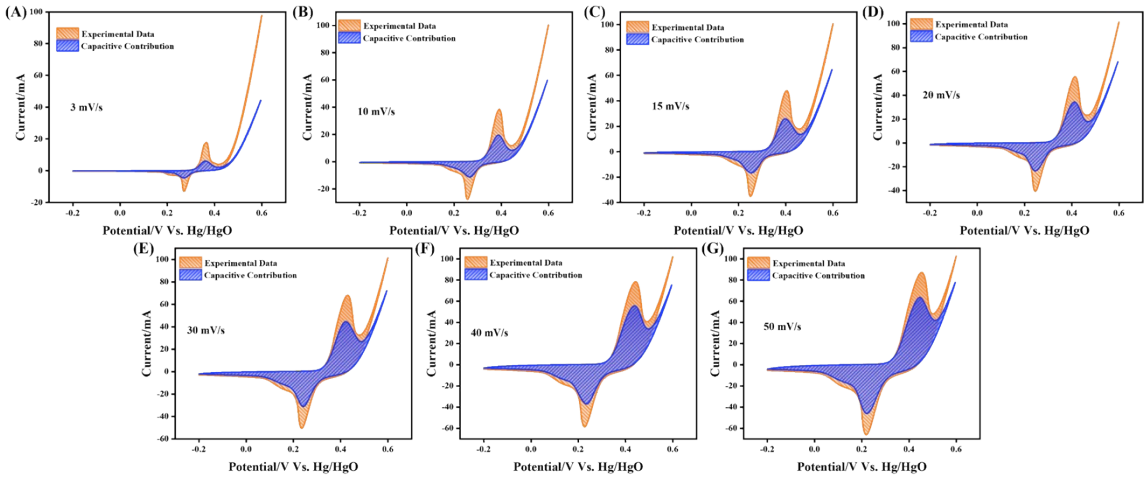

Fig. S2: (A-G) Capacitive and diffusive CV of NPCA0.3 electrodes at different scan rates of 3 to 50 mV/s.

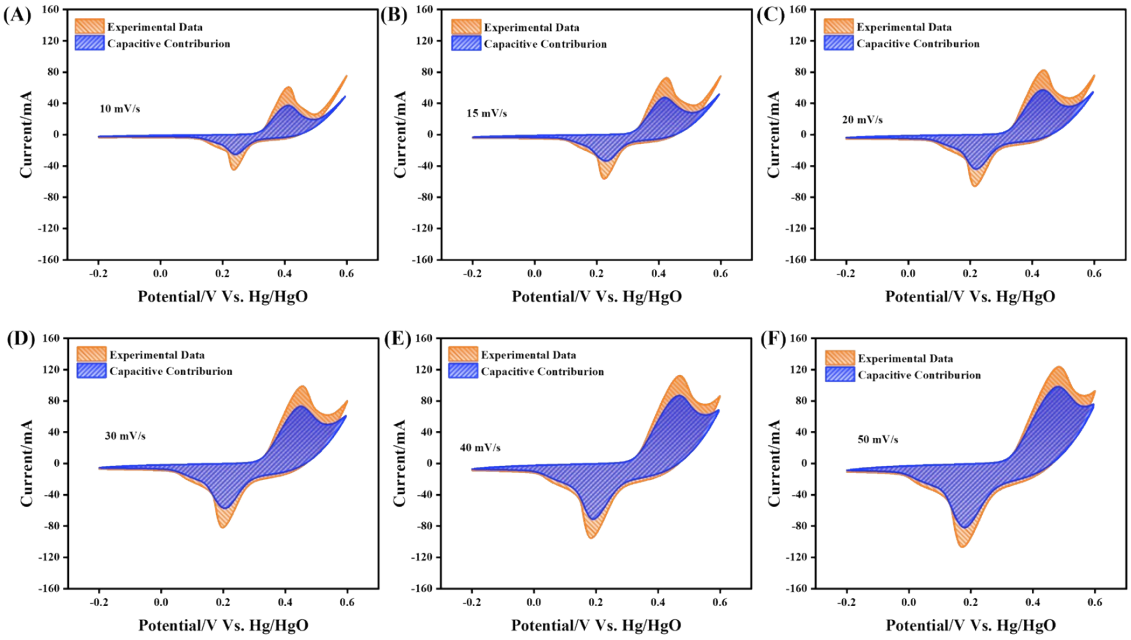

Fig. S3: (A-F) Capacitive and diffusive CV of NPCA0.5 electrode at different scan rates of 10 to 50 mV/s.

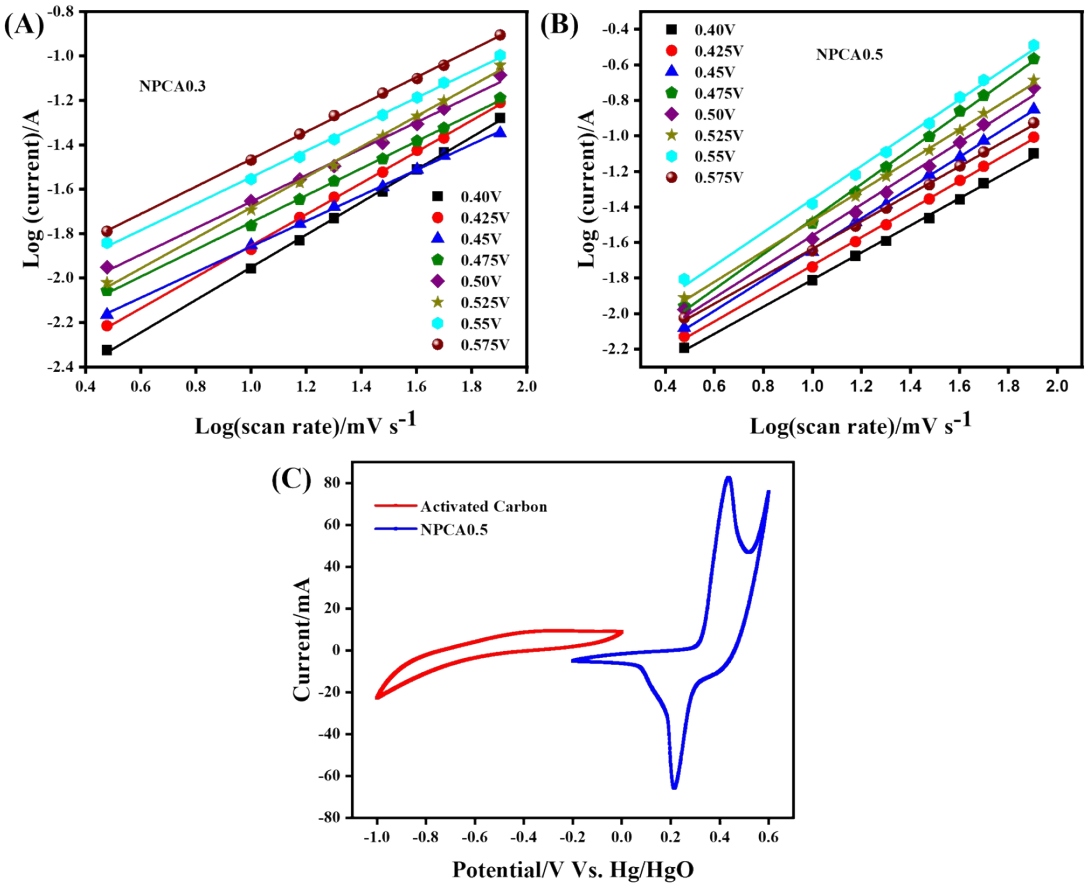

Fig. S4: Calculated b values at different potentials of (A) NPCA0.3, (B) NPCA0.5 and (C) CV analysis of NPCA0.5 and AC at scan rate of 20 mV/s.

Table S1: Specific capacitance and capacity of NP. NPA0.3, and NPA0.5 at different scan rates of 3 to 80 mV/s.

Scan Rate (mV/s)	Specific Capacitance (F/g)			Specific Capacity (C/g)		
3	1090.1	791.4	2034.8	872.1	633.1	1627.8
10	856.9	646.9	1486.0	685.5	517.6	1188.8
15	779.5	616.4	1348.6	623.6	493.1	1078.9
20	721.1	585.3	1256.6	576.9	468.3	1005.2
30	642.5	542.1	1126.7	514.0	433.7	901.4
40	582.8	509.5	1025.3	466.3	407.6	820.2

50	534.9	482.7	939.9	427.9	386.2	751.9
80	452.5	424.1	755.4	362.0	339.3	604.2

Table S2: Specific capacitance value with previous reported works.

No.	**Electrode Name**	**Specific Capacitance**	**Scan Rate/Current Density**	**Ref.**
1	FeNiC/rGO	1510.5 F/g	--/2 A/g	[3]
2	P-CuCo2O4	1260.0 F/g	--/1 A/g	[4]
3	SWCNTs/C1Z1S	1750 F/g	10 mV s^{-1}/--	[5]
4	FCP3	1950 F/g	10 mV s^{-1}/--	[6]
5	NP450-100 AC	2009.8	--/1 A/g	[7]
6	NiP-6	1192 F/g	10 mV s^{-1}/--	[8]
7	CMVC-4	1848.6 F/g	--/2 A/g	[9]
8	Mn0.5Co0.5(HPO4)	1727 F/g	--/1 A/g	[10]
9	NPO-30	1535 C/g	5 mV s^{-1}/--	[11]
10	Ni-Co-P80	1916.9 F/g	5 mV s^{-1}/--	[12]
11	NiCoNPO	1835 F/g	5 mV s^{-1}/--	[13]
12	NPCA0.5	2034 F/g	3 mV s^{-1}/--	This Work

Table S3: Specific capacitance and capacity of NP. NPA0.3, and NPA0.5 at different current densities of 1 to 15 A/g.

Current Density (A/g)	**Specific Capacitance (F/g)**			**Specific Capacity (C/g)**		
1	758.8	455.5	1067.6	455.3	273.3	640.5
2	670.3	431.3	1013.0	402.2	258.8	607.8

3	620.0	418.5	899.5	372.0	251.1	539.7
4	590.7	408.0	858.0	354.4	244.8	514.8
5	544.0	376.0	795.0	326.4	225.6	477.0
8	485.3	364.0	776.0	291.2	218.4	465.6
10	421.7	366.7	718.3	253.0	220.0	431.0
15	342.5	250.0	637.5	205.5	150.0	382.5

Table S4: Discharging time of NP. NPA0.3, and NPA0.5 at different current densities.

Current Density (mV/s)	**Discharging Time (Sec)**		
1	455.3	273.3	640.5
2	201.1	129.4	303.9
3	124	83.7	179.9
4	88.6	61.2	128.7
5	54.4	37.6	79.5
8	36.4	27.3	58.2
10	25.3	22	43.1
15	13.7	10	25.5

Table S5: Ragone plot comparative study of current work and previous reported work.

Electrode Type	**Specific Capacitance (F/g)**	**Energy Density (Wh/kg)**	**Power Density (W/kg)**	**Stability/ Cycles**	**Ref.**
$Ni_2Mn(PO_4)_2.8H_2O$	163.1	66.22	400	81%/15k	[14]
NCP//AC	144.7	45.2	749.9	70%/10k	[15]
NCPCA//AC	163	10.8	749	88%/5k	[16]

NiCo-P/$Ni_3V_2O_8$//AC	208	65	750	84.2%/10k	[17]
AC//YS-CNHP	143.1	50.9	800	69.5%/10k	[18]
NV_2O_5@CoS//AC	178.4	71.6	849.8	90.6%/10k	[19]
$MnCo_2O_4$@NiMo-LDH	116.1	43.2	815.8	71%/5k	[20]
S-CNP5//PVA-KOH//rGO	120	42.59	1600	90%/5k	[21]
$Cu_2P_2O_7$//AC	167.6	39.5	1086	-	[22]
P-$CoNi_2Se_4$/$Ti_3C_2T_x$//AC	105.1	37.4	800	80%/5k	[23]
FeP@CNTF//Ni_2P@CNTF	191.1	67.9	800	69.4%/10k	[24]
MnP_6Mo_{18}@PCNFs//AC	188.2	71.2	830.1	93%/10k	[25]
NPCA0.5//KOH//AC	**228.1**	**81.1**	**1146.1**	**92.3%/6k**	**Current**

1. Iqbal, M.Z., U. Abbasi, and M. Alzaid, *Cobalt manganese phosphate and sulfide electrode materials for potential applications of battery-supercapacitor hybrid devices.* Journal of Energy Storage, 2022. **50**: p. 104632.
2. Ye, H., et al., *Advanced MXene/graphene oxide/lignosulfonate inks for 3D printing thick electrodes with vertically aligned pores to dually boost mass loading and areal capacitance.* Advanced Functional Materials, 2025. **35**(3): p. 2413343.
3. Pan, H., et al., *Metal organic framework derivatives as matched positive and negative electrodes for high energy and power density asymmetric supercapacitors.* Journal of Energy Storage, 2026. **149**: p. 120427.
4. Fan, L., et al., *Study of phosphorization effect on urchin-like CuCo2O4 cathodes for high-performance supercapacitors.* Journal of Alloys and Compounds, 2025. **1010**: p. 177362.
5. Hamayun, U., et al., *Optimization of the redox-active copper zinc sulfides with the integration of SWCNTs nanocomposites for the asymmetric supercapacitor.* Journal of Power Sources, 2026. **672**: p. 239572.
6. Sutar, P., P. Deshmukh, and A. Kadam, *Enhanced electrochemical performance of Fe doped CoCuP electrodes: Derived 3D nanopetals for supercapacitor application.* Journal of Energy Storage, 2026. **146**: p. 120150.
7. Fan, L., et al., *Efficient synthesis of high-performance nickel phosphide cathodes for supercapacitors and insights into charge storage dynamics.* Journal of Energy Storage, 2026. **145**: p. 119802.
8. Yadav, A.A., et al., *Enhanced asymmetric supercapacitor performance using 2D Ni2P2O7 nanoplates with high specific capacitance.* Journal of Energy Storage, 2026. **161**: p. 121717.
9. Katkar, P.K., S.-H. Chun, and S.-W. Lee, *Rational design and electrochemical characterization of a 3D cobalt phosphate/MXene/vertical graphene nanohills (VGNHs) heterostructure for supercapacitor applications.* Journal of Alloys and Compounds, 2026. **1050**: p. 185907.
10. Ahn, K.-S., et al., *A high-performance asymmetric supercapacitor consists of binder free electrode materials of bimetallic hydrogen phosphate (MnCo(HPO4)) hexagonal tubes and graphene ink.* Electrochimica Acta, 2022. **426**: p. 140763.

11. Aldayyat, A., F.K. Yam, and M.D.J. Ooi, *Nickel phosphate/graphene oxide with excellent performance for asymmetric supercapacitor.* Diamond and Related Materials, 2026. **161**: p. 113165.
12. Li, H., et al., *Phosphate ion-functionalized nickel-cobalt layered double hydroxide nanosheets derived from metal-organic framework compounds for high-performance asymmetric supercapacitors.* Journal of Alloys and Compounds, 2023. **935**: p. 167876.
13. Mohanty, R.I., et al., *Hybrid bimetallic phosphonates as cathode materials for miniaturized in-plane asymmetric supercapacitor device.* Journal of Energy Storage, 2024. **80**: p. 110313.
14. Li, M., et al., *Rational design of crystalline/amorphous nickel manganese phosphate octahydrate heterostructure for high-performance aqueous and all-solid-state asymmetric supercapacitors.* Chemical Engineering Journal, 2024. **482**: p. 148895.
15. Thilagasubbulakshmi, A. and P. Sivakumar, *Facile synthesis of nickel–cobalt phosphate binary nanocomposite with an enriched electrochemical performance for asymmetric supercapacitor applications.* Journal of Materials Science: Materials in Electronics, 2024. **35**(22): p. 1551.
16. Mustafa, M.N., et al., *Chronoamperometric optimisation of bimetallic nickel-cobalt phosphate electrodes for dual-function electrochromic supercapacitors.* Journal of Power Sources, 2025. **658**: p. 238327.
17. Hao, Y., et al., *Highly dispersive nickel vanadium oxide nanoparticles anchored on nickel cobalt phosphate micron-sheets as cathodes for high-energy hybrid supercapacitor devices.* Journal of Alloys and Compounds, 2025. **1010**: p. 177893.
18. Jia, X., et al., *Controllable construction of porous yolk shell phosphate-functionalized Co/Ni-layered double hydroxides for high-performance supercapacitor.* Electrochimica Acta, 2025. **537**: p. 146853.
19. Zhou, W., et al., *Guiding nitrogen doped vanadium pentoxide nanoclusters on cobalt sulfide nano-flakiness as stable seamless interface anode toward highly energy density and durable asymmetric supercapacitors.* Journal of Colloid and Interface Science, 2025. **679**: p. 531-543.
20. Wu, Y., et al., *Core-shell manganese cobalt oxide-nickel molybdenum layered double hydroxide composites for supercapacitor electrodes.* Journal of Energy Storage, 2025. **131**: p. 117529.
21. Patil, V.V., et al., *Crystallinity transformation engineering of hydrous cobalt nickel phosphate cathodes for hybrid supercapacitor devices: Extrinsic/battery to intercalation type pseudocapacitors.* Chemical Engineering Journal, 2024. **485**: p. 150055.
22. Mendhe, A.C., et al., *Hierarchically structured Cu2P2O7 nanoflakes as a binder-free electrodes for high-performance supercapacitors.* Chemical Engineering Journal, 2024. **496**: p. 153857.
23. Hu, M., et al., *Boosting electrochemical activity via manipulating the d-band center of CoNi2Se4/MXene heterostructure for supercapacitor application.* Chemical Engineering Journal, 2025. **513**: p. 162785.
24. Zhong, H., et al., *Iron phosphide/carbon nanotube composite with high-performance and decoupled areal capacity as negative electrodes for asymmetric supercapacitors.* Chemical Engineering Journal, 2025. **509**: p. 161278.
25. Wang, M., et al., *Construction of nanocomposite by anchoring basket-like Polyoxometalate on porous carbon nanofibers for enhance electrochemical energy storage and bifunctional biosensing performance.* Chemical Engineering Journal, 2025. **513**: p. 162840.